Separation Science and Technology
Publication details, including instructions for authors and subscription information:
http://www.informaworld.com/smpp/title~content=t713708471

A Computer Simulation of Linear Gel Permeation Chromatography

A. C. Ouano[a]; J. A. Barker[a]
[a] IBM RESEARCH LABORATORY, SAN JOSE, CALIFORNIA

To cite this Article Ouano, A. C. and Barker, J. A.(1973) 'A Computer Simulation of Linear Gel Permeation Chromatography', Separation Science and Technology, 8: 6, 673 — 699
To link to this Article: DOI: 10.1080/00372367308056063
URL: http://dx.doi.org/10.1080/00372367308056063

SEPARATION SCIENCE, 8(6), pp. 673–699, 1973

A Computer Simulation of Linear Gel Permeation Chromatography

A. C. OUANO and J. A. BARKER

IBM RESEARCH LABORATORY
SAN JOSE, CALIFORNIA 95193

Abstract

A phenomenological model based on a set of partial differential equations and boundary conditions is proposed for chromatography and, in particular, for gel permeation chromatography. The intractable boundary value problem, which does not have a closed form solution, was handled through the use of numerical methods employing a very large and very fast computer (IBM 360/195). The chromatograms generated by the computer simulator were compared with experimental chromatograms of various molecular weight polymers. The computer generated overlay plots of the simulated and experimental chromatograms showed good agreement (the two plots almost superimposed). The effect of other parameters on the chromatogram, i.e., flow rate, stationary phase bead size, solute diffusion coefficient in the stationary and mobile phases, and the partition coefficient were also investigated.

INTRODUCTION

As Giddings and Eyring pointed out (*1*), the general solution to the chromatographic equation is not possible in a practical sense. Other investigators (*2–6*) have also found this to be true. Most of the difficulty lies in obtaining a closed form solution of the general chromatographic equations. Present availability of high-speed computers circumvents the above difficulty, since solutions to very complex problems can be obtained by numerical analysis methods to a high degree of precision.

The model chosen in this work is a phenomenological one. It uses a set of partial differential equations and boundary conditions which de-

scribe the behavior and fate of the molecule being fractionated in a volume element of the chromatographic column. The column volume element is composed of the stationary and the mobile phases where equilibria and transport processes take place. As such, the model is of general nature and can be used to simulate a broad class of column chromatography (gas–liquid, liquid–liquid, and gel permeation or gel exclusion chromatography). For the present the simulation is limited to the specific area of gel permeation chromatography (GPC), which is one of the most complex chromatographic processes.

The practical objective of this work was to determine the effect of the various material and experimental parameters on the band spreading or zone dispersion of the chromatographic peaks. The particular material and experimental parameters studied are the following:

Material parameters

1. Molecular weight of the material being fractionated.
2. Stationary phase characteristics, i.e., bead size and permeability characteristics.

Experimental parameters

1. Flow rate.
2. Packing efficiency, i.e., effect of eddy diffusivity.

The fidelity of the simulation is verified by comparison with experimental results. Since the stationary phase characteristics and packing efficiency are difficult to vary and control experimentally, the effect of molecular weight was the only parameter in which the model was compared with experiment. The comparison between experimental and simulated chromatographs for various flow rates will be a subject of future study.

THE MODEL

In high-resolution chromatography, of which analytical GPC is considered to be one type, the dimensional characteristics of the column and that of the stationary phases are: $R_0/R_1 < 10^{-2}$ and $R_0/L < 10^{-4}$, where R_0 and R_1 are the stationary phase bead and column radii, respectively, and L is the column length. As a means of comparison, if the letters on this page represent the bead radius, the column radius is twice the width of this page and the column length is over 100 feet. Scanning electron (SEM) photomicrographs shown in Fig. 1 and 1a indicate that

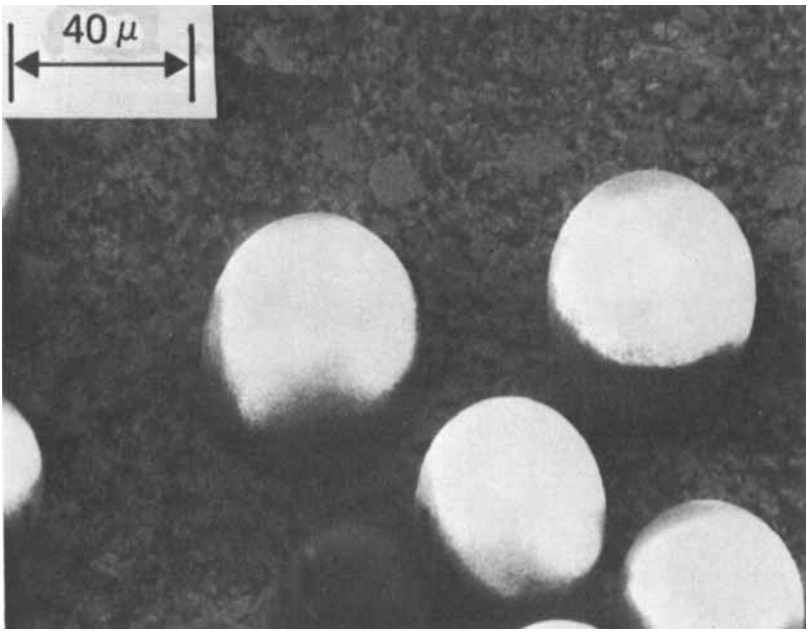

FIG. 1. SEM photomicrograph showing the uniform size and spherical shape of Styragel beads.

the stationary phase is almost spherical in shape and the bead surface is covered with irregularly shaped pores with a wide size distribution. The average pore size to bead radius ratio is less than one ten-thousandth ($R_p/R_0 < 10^{-4}$).

The very small ratio of bead to column radius is fortunate, for it makes the representation of the packed column by a lumped parameter model a valid assumption. That is, the column can be represented by two continuous phases, the stationary and the mobile. If we further assume that the beads are homogeneously packed throughout the column, i.e., the interstitial space between beads are uniform in size and shape, then a single channel model representation of the packed column is adequate.

The fractionating column is described as a region in which the solute concentration varies in two spatial dimensions, x (measured along the column) and y (measured transversely to the flow). We shall idealize the geometry by supposing the moving phase to be between the planes $y = 0$ and $y = l_m$, and the stationary phase to lie between $y = l_m$ and $y =$

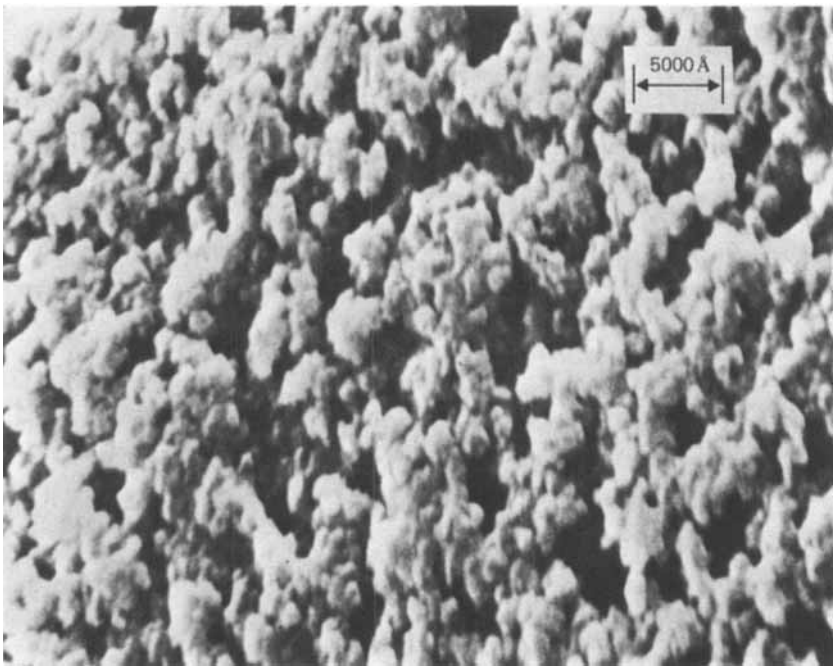

FIG. 1*a*. High magnification SEM photomicrograph showing the pores and fine structures of the Styragel beads.

$l_m + l_s$; here l_m and l_s may be regarded as effective film thicknesses. The material balance equations and boundary conditions describing the system are shown in Scheme 1 in which c_m and c_s are concentrations in the moving and stationary phases, respectively; D_m and D_s are the corresponding diffusion coefficients; D_e is the eddy diffusion coefficient; and u is the velocity of the moving phase.

The mobile phase material balance equation is

$$\frac{\partial c_m}{\partial t} + u\frac{\partial c_m}{\partial x} = D_e\frac{\partial^2 c_m}{\partial x^2} + D_m\frac{\partial^2 c_m}{\partial y^2} \tag{1}$$

The stationary phase material balance equation is

$$\frac{\partial c_s}{\partial t} = D_s\frac{\partial^2 c_s}{\partial y^2} \tag{2}$$

The boundary and initial conditions are

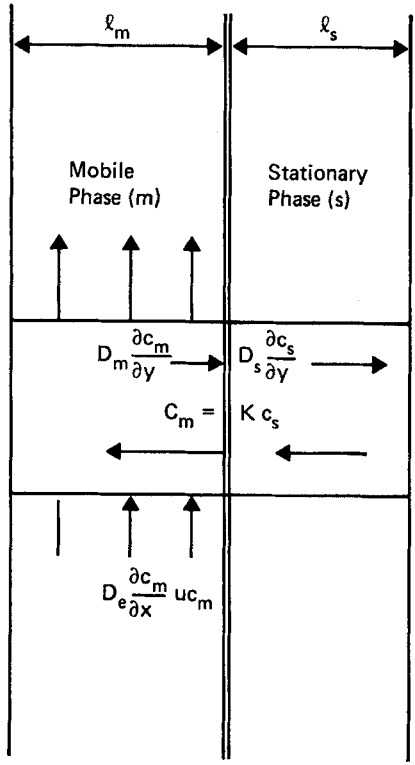

SCHEME 1. Single channel GPC model.

$$c_m = \frac{q}{l_m}\delta(x) \qquad (t = 0, 0 < y < l_m) \tag{3}$$

$$c_s = 0 \qquad (t = 0, l_m < y < l_m + l_s) \tag{4}$$

$$c = K_i c_m \qquad (\text{all } x, t; y = l_m) \tag{5}$$

$$D_m \frac{\partial c_m}{\partial y} = D_s \frac{\partial c_s}{\partial y} \qquad (\text{all } x, t; y = l_m) \tag{6}$$

$$\frac{\partial c_m}{\partial y} = 0 \qquad (\text{all } x, t; y = 0) \tag{7}$$

$$\frac{\partial c_s}{\partial y} = 0 \qquad (\text{all } x, t; y = l_m + l_s) \tag{8}$$

This is a picture of a lumped parameter model which represents the fractionating column by a mobile phase in which the solute undergoes molecular and eddy diffusion, and by a stationary phase where the solute molecules undergo partition and diffusion. Eddy diffusion in the mobile phase is a consequence of the "mixing" of the mobile phase as it flows around the individual column packing beads (stationary phase). The model assumes that there is no bulk velocity or solute concentration gradient in the radial direction of the column. Within most chromatographic experimental conditions where fingering and severe velocity profile distortion across the column is absent, this physical description of a GPC column holds true.

In Eq. (5), K_i represents a partition coefficient, in Eq. (3) it is assumed that the sample is introduced as a sharp pulse, hence, $\delta(x)$ is the Dirac delta function, and q is a normalizing constant which determines the total amount of material injected (q is the amount injected per unit "width" of the column in the third space dimension). Equations (5) and (6) express the conditions of equilibrium and conservation of flux at the interface, while Eqs. (7) and (8) ensure that there is no flux out of the system at $y = 0$ and $y = l_m + l_s$.

To solve this boundary-value problem we define the Laplace-Fourier transform by

$$\hat{\bar{c}}(k,p,y) = (2\pi)^{-1/2} \int_0^\infty e^{-pt}\, dt \int_{-\infty}^{\infty} e^{ikx}\, dx\, c(x, t, y) \tag{9}$$

In terms of c_m and c_s, Eqs. (1)–(8) become ordinary differential equations which can be solved analytically. The quantity of direct interest is the total flux F at the column exit, defined by

$$F(x, t)\big|_{x=L} = \int_0^{l_m} \left(u c_m - D_E \frac{\partial c_m}{\partial x} \right)_{x=L} dy \tag{10}$$

where L is the length of the column.

The transform of this quantity is found to be given by

$$\hat{\bar{F}} = \frac{q(u + ikD_E)}{\sqrt{2\pi}(p - iku + k^2 D_E)} \left\{ 1 - \frac{S}{T[\alpha T \coth S + S \coth T]} \right\} \tag{11}$$

where

$$S = (p l_s^2 / D_s)^{1/2} \tag{12}$$

$$T = [(p - iku + k^2 D_E) l_m^2 / D_m]^{1/2} \tag{13}$$

and

$$\alpha = K_i D_m l_s / D_s l_m, \qquad K_i = 1/K \tag{14}$$

The inverse of the transform (11) cannot be found in closed form. To perform the Laplace inversion we evaluated the first six *moments* (with respect to time t) of $\exp[-p_0 t_{F(t)}]$, according to the equation (in which $\bar{F}$ denotes the *Laplace* transform)

$$(-1)^m \frac{\partial^m}{\partial p^m} \bar{F}|_{p=p_0} = \int_0^\infty \exp(-p_0 t)\, t^m F\, dt \tag{15}$$

We then fitted these moments to an expression of the form

$$F \exp(-p_0 t) = t^{-3/2} \exp(-\mu t - \nu/t)[\sum_{i=0} a_i t^i]. \tag{16}$$

This form is capable of describing approximately Gaussian peaks with high accuracy, and has the advantage of providing the *exact* solution in several limiting cases (complete equilibrium, D_m, $D_s \to \infty$; no penetration into the stationary phase, $D_s \to 0$). The value of p_0 is arbitrary, provided that it is not chosen too large; however, one cannot choose $p_0 = 0$ because divergent integrals over k arise.

The Fourier inversion was performed by direct numerical integration using Filon quadrature with complex arithmetic and automatic error control. The accuracy of this procedure was checked by comparing with analytic solutions for the case of complete equilibration and by using different numbers of moments and different values of p_0 in other cases. The accuracy was found to be satisfactory even for severe deviations from Gaussian behavior ("tailing" of peaks). Further details of the derivation of Eqs. (11)–(14) and of the numerical procedure will be given in a separate report.

In reality, the stationary phase beads are not packed uniformly in the column but, rather, exist as regions of varying packing density. This implies that the interstitial spaces (flow channels in the column) have a size distribution. Since the curvature of the column wall is different from that of the beads, it is expected that most of the "lesser" packed regions (larger and longer channel) exist near the column wall/stationary phase interface. This packing inhomogeneity results in a nonuniform velocity profile across the column radius (channeling effect). The average size and size distribution of these interstitial spaces will depend on the packing technique, the size distribution of the stationary phase beads, the bead to column radius ratios, and the tendency of the stationary phase beads to

form agglomerates (this becomes more of a problem as bead radius becomes less than 20 μ). For a "well-packed column" with narrow bead size distribution without agglomeration, a value of interstitial volume fraction of 0.364 (theoretical volume fraction for a randomly packed column) is usually approached.

The channeling phenomenon which manifests as forward skewing ("bearding") in chromatograms is usually not a problem with a "well-packed column" at relatively low flow rate. But as flow rate increases (increasing pumping pressure), the bearding problem becomes a more important component of zone broadening in chromatograms. A single channel model which assumes a homogeneous column packing (a flat velocity profile across the column) is not adequate, for it will not predict forward skew with increasing flow rate. Consequently, it is expected that increased discrepancy between experiment and the single channel model will result in high flow rate chromatography.

MULTICHANNEL MODEL

In this model the inhomogeneity of column packing is taken into account by representing a column with channels of varying interstitial cross section and length. The channels are largest and longest near the column wall and decrease in size toward the column axis. To take into account the mass transfer due to eddy and molecular diffusion between channels, the column in the axial direction is divided into several channel lengths, i.e., l_c (length of a channel) = 50 dp, here dp = bead diameter. Mixing (mass interchange between channels) is allowed to take place between the channel sections at the end of each channel length. The multichannel representation of a column is analogous to a semicrystalline solid, i.e., crystalline regions representing channels and amorphous regions representing "mixing" regions.

In this way the chromatogram of the model can be evaluated as a convolution of all the retention volume distributions of the N number of parallel channels (radial) with M sections (axial) which represent the column. In principle, a chromatogram using the multiple channel model can be handled by very fast computers. However, we have elected to use the single channel model, although perhaps less precise, as our first involvement in chromatographic simulation.

NORMALIZING PARAMETERS

In order to reduce the important material and experimental parameters

into proper dimensions, i.e., compatible with the parameters of the single channel model, several important dimensional parameters are determined. These dimensional parameters are based on the average physical characteristics of the fractionating columns.

If we consider the diffusion layer thickness in the mobile phase, l_m, as the interstitial volume V_0 divided by the total surface of the stationary phase as a reasonable assumption, then it can readily be shown that

$$l_m = \Phi_m R_0/3(1 - \Phi_m) \tag{17}$$

The accessible volume per stationary bead to a molecule with a partition coefficient K is

$$V_a/N_b = KV_I/(V_I/\Phi_s(4/3)\pi R_0^3) \tag{18}$$

If $l_s = R_0 - R$ is the thickness of the diffusion layer of the solute in the stationary phase, then

$$V_a/N_b = \Phi_s(4/3)\pi(R_0^3 - R^3) \tag{19}$$

Combining Eqs. (18) and (19), we obtain for the diffusion layer thickness in the stationary phase

$$l_s = R_0(1 - \sqrt[3]{1 - K}) \tag{20}$$

Φ_m and Φ_s are the interstitial volume fraction of the column and the internal volume fraction of the bead ($\Phi_s = V_I/V_b$, where V_I bead volume accessible to solvent or monomer and V_b is the bead volume). R_0 is the stationary phase bead radius, and N_b is the number of bead in the column.

The interstitial velocity U, the mean interstitial residence time T_i, and column length L are simply computed as follows:

$$U = Q/(\Phi_m \pi R_1^2) \tag{21}$$

$$T_i = L/U \tag{22}$$

$$L = V_T/\pi R_1^2 \tag{23}$$

where V_T is the total volume of the column (interstitial volume + bead volume), Q is the flow rate, and R_1 is the column radius.

EXPERIMENTAL

The success of a model can best be judged by its ability to mimic actual chromatographic experiments wherein the experimental as well as the

material parameters have been precisely determined. In testing the model, a chromatograph was designed in such a manner that extra column dispersion due to plumbing, sample injection, and detector had been minimized. In this chromatograph the inlet and outlet of the fractionating column were connected directly to a septum injection system and a Water's Associates differential refractometer detector (Model R401). The septum injection system had a total mixing volume of less than 15 μl. The Water's Associates Model M-6000 solvent delivery system was used.

A 0.307-in. i.d. stainless steel column 4 ft in length was packed with Styragel stationary phase (60 μ average bead diameter) obtained from Water's Associates. SEM photomicrograph of the bead and its surface are shown in Figs. 1 and 1*a*. A "balance mix" column packing technique using a nitrogen bottle to supply a packing pressure up to 1000 psi was used. The balance mix was a suspension of the stationary phase in a mixture of perchloroethylene and acetone. A sketch of the packing apparatus is shown in Fig. 2.

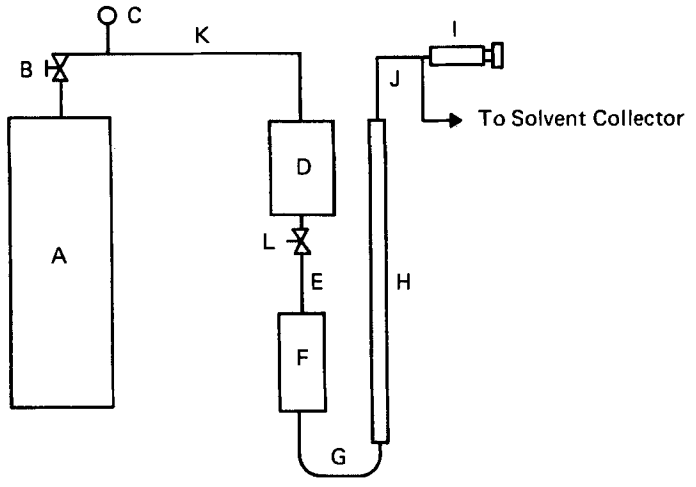

A – N_2 Cylinder
B – Pressure Regulator
C – Pressure Gauge
D – 1000 ml High Pressure Vessel
E – High Pressure S.S. Hose
F – 500 ml High Pressure Vessel
G – 1/4" S.S.U-Tube Connector
H – Column to be Packed
I – Syringe
J – 1/16" Teflon Tubing
K – 1/8" S.S. Tubing
L – Ball Valve

FIG. 2. A schematic diagram of the high pressure column packing system using the balance mixed method.

The resulting packed column had the following attributes in chloroform at room temperature with ethyl benzene as solute:

Column efficiency: 1080 plates/ft.
Interstitial volume fraction (Φ_m) = 0.364.
Bead accessible volume fraction (Φ_s) = 0.616 (accessible to ethylbenzene).
Permeability limit: 600,000 (polystyrene molecular weight).

The calibration curve for this polystyrene sample is shown in Fig. 3. The value of Φ_m = 0.364 is very close to the interstitial volume of randomly packed rigid spheres predicted by LeFevre (*7*) and experimentally verified by Scott (*8*).

To provide a high degree of precision in reducing the experimental chromatogram into normalized retention volume distribution curves and to obtain accurate variance and standard deviation measurements, the

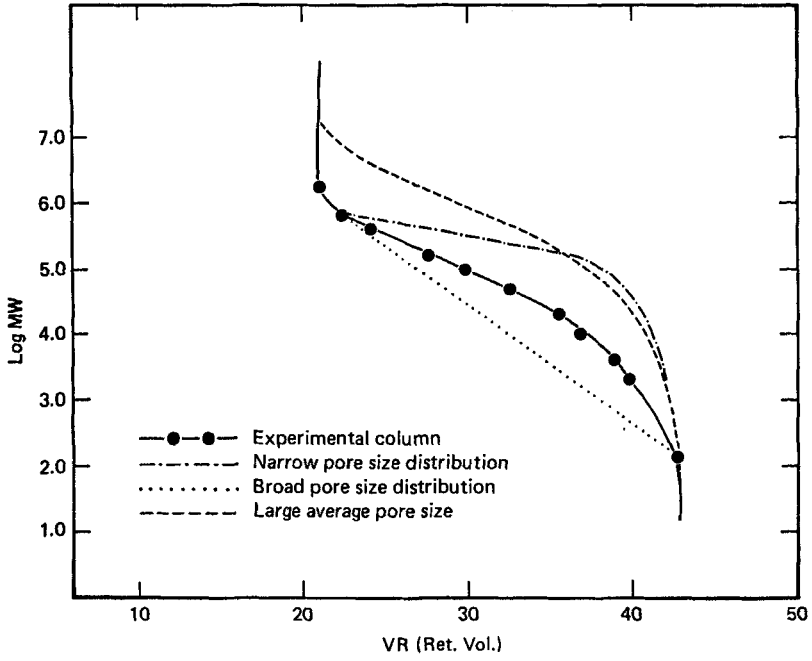

FIG. 3. Calibration curves of the actual experimental fractionating column and hypothetical columns with various pore size averages and distributions.

chromatograph was coupled to an IBM System/7 sensor based computer for data acquisition and an IBM 360/195 computer for data reduction. Simpson's rule was used for peak area integration. Figure 4 shows a schematic of this system. A detailed description of this laboratory automation system will be given in a future publication.

Simulation Parameters and Their Physical Meaning

It is evident from the SEM photomicrographs that the pore shape and size distribution is too irregular to provide a direct relationship between partition coefficient and the physical dimension of the pore. Hence a more practical approach in relating bead characteristics and polymer solute molecular weight with partition coefficient was taken. The stationary phase pore properties were characterized through the shape of its calibration curve (plot of polystyrene standard vs its retention volume) and the diffusivity of the polymer solute in the stationary phase. At constant bead accessible volume and permeability limit, the slope of the calibration

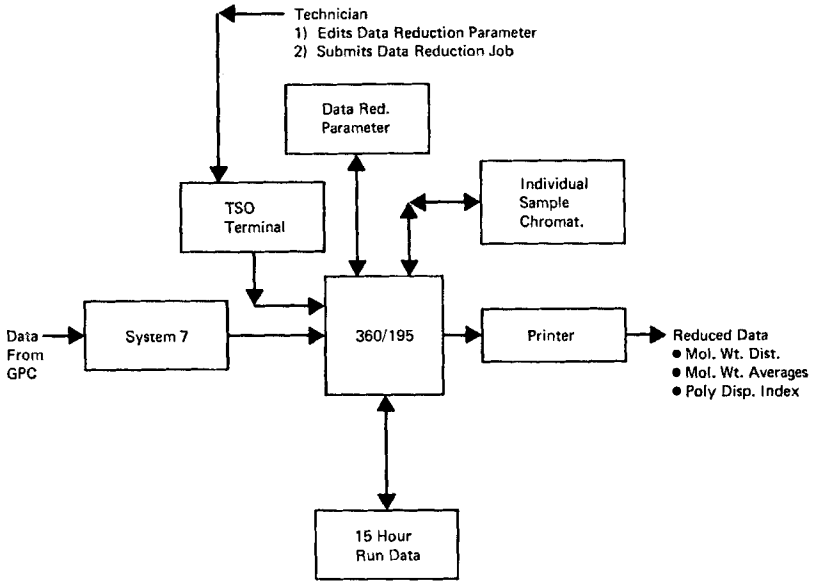

FIG. 4. A schematic flow diagram of the data reduction procedure of GPC chromatograms.

curve is proportional to the pore size distribution. The shape and surface characteristics of the pore are reflected by the diffusivity of the solute in the stationary phase. In view of the present knowledge of GPC, the above characterization of the stationary phase is considered reasonable. Consequently, the fundamental parameters of the phenomenological model can be expressed with experimentally measurable material and experimental parameters of GPC.

The partition coefficient of the polymer in a stationary phase is related to its molecular weight via its calibration curve and the relationship:

$$V_R = V_T[\Phi_m + K\Phi_s] \tag{24}$$

and

$$V_R = f(\mathrm{MW}) \qquad \text{(obtained from Fig. 3)} \tag{25}$$

where V_R is the retention volume of polymer with molecular weight MW. V_T is the total volume of the column (the total volume of the fractionating column was measured to be 58.23 ml).

Equations (24) and (25) provide a means by which the partition coefficient K can be calculated for any molecular weight polymer when the column calibration curve is known.

The diffusion coefficients of the solute in the mobile D_m and stationary D_s phases are calculated using

$$D_m = J/M^{\alpha_m} \tag{26}$$

$$D_s = J/M^{\alpha_s} \tag{27}$$

α_m and α_s were obtained from literature (*9*, *10*) values as 0.60 and 1.00, respectively. J was determined to be 5×10^{-4} from diffusion values of ethylbenzene in $CHCl_3$ at room temperature.

Eddy diffusion in packed columns has been studied by several investigators (*11–13*). Klinkenberg and Sjenitzer (*11*) showed that the eddy diffusivity D_E can be expressed in terms of the diameter of the stationary phase beads d_p and the average interstial velocity U:

$$D_E = \lambda d_p U \tag{28}$$

λ is the packing efficiency constant which has been determined experimentally (*11*) to have a value between 1 to 4.

Having defined the input variables of the model in terms of experimentally determined and literature reported parameters, Table 1, a

TABLE 1

Parameters Used in the Computer Simulation

$R_0 = 30\ \mu$	$V_T = 58.23$ ml
$R_1 = 0.307$ in.	$J = 5 \times 10^{-4}$
$\Phi_m = 0.364$	$\alpha_m = 0.60$
$\Phi_s = 0.616$	$\alpha_s = 1.04$
$Q = 1$ ml/min	$\lambda = 2.00$

simulated chromatogram, can now be computed and compared with an experimental GPC chromatogram.

DISCUSSION OF RESULTS

Figure 5 shows computer-generated overlay plots of simulator-generated chromatograms and the normalized experimental retention volume distributions of ethylbenzene and a polystyrene (PS-160,000) calibration standard. It is evident from Fig. 5 that both the width (standard deviation) and skew of the simulated chromatogram is very sensitive to the value of the exponent (α_s) of the diffusion/molecular weight relationship in the stationary phase. The best agreement between the simulated chromatogram and the experimental retention volume distribution was obtained when the value of α_s was between 1.00 and 1.10. A slight displacement between the peaks of the simulated and experimental chromatogram of ethylbenzene is also evident. This is due to the difficulty in obtaining (by linear interpolation) a precise value of the partition coefficient K for ethylbenzene, which lies in the very nonlinear region of the calibration curve in Fig. 3. This difficulty is not serious in the case of the partition coefficient of PS-160,000, which is located in the linear portion of the calibration curve. Although both simulated and experimental chromatograms were obtained for a complete range of molecular weights (PS 1.8×10^6 to ethylbenzene), only those of PS-160,000 and ethylbenzene were overlayed as complete chromatograms. This was done to eliminate congestion in Fig. 5. The characteristics of the simulated and experimental chromatograms for the complete range of molecular weights were, however, compared by plotting variances (characterizing the band broadening) of the distribution as a function of molecular weights as shown in Fig. 6.

Figure 6 shows an unexpected maximum in the dependence of the variance of the chromatogram on solute molecular weight. For the column tested (packed with 10^4 permeability limit for a gel), the plot shows a variance maximum between 51,000 and 97,200 polystyrene molecular

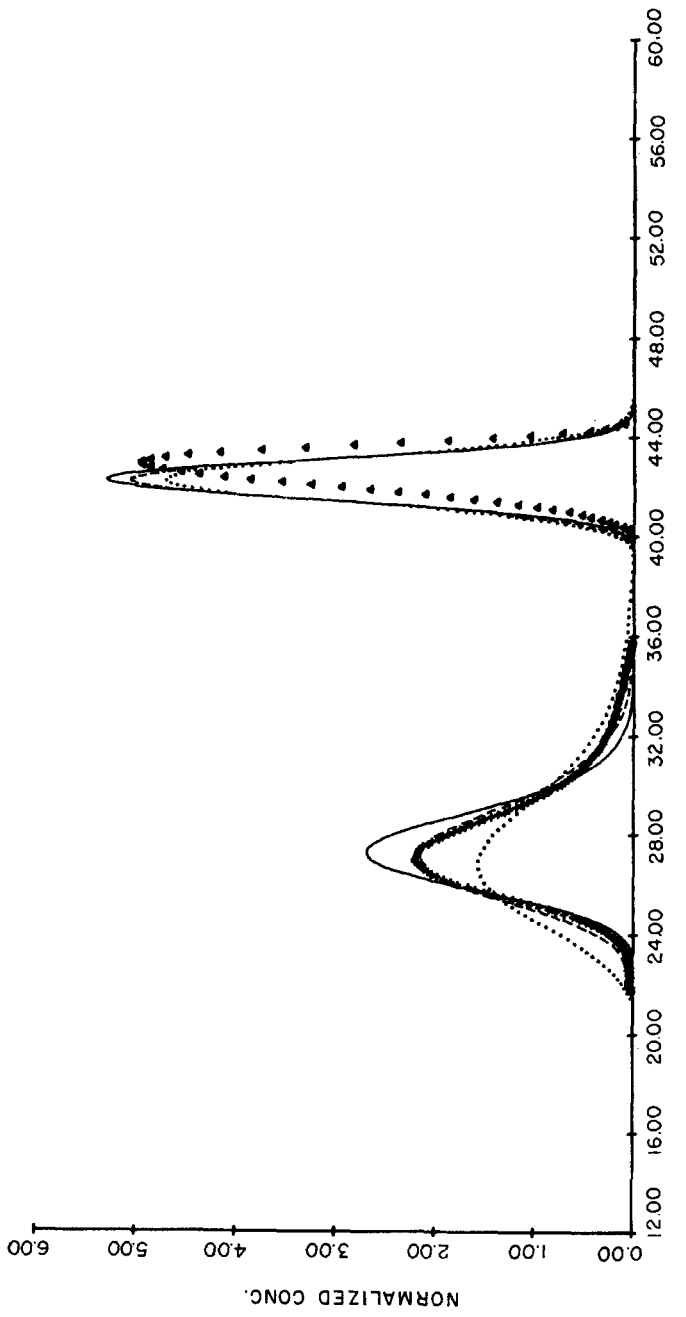

FIG. 5. Computer overlay plot of the experimental and simulated retention volume distribution shows good agreement between experimental and computer simulation results. + and ▲ are experimental points; (—) $\alpha_s = 1.0$, (- -) $\alpha_s = 1.04$, and (••) $\alpha_s = 1.10$ are simulated chromatograms.

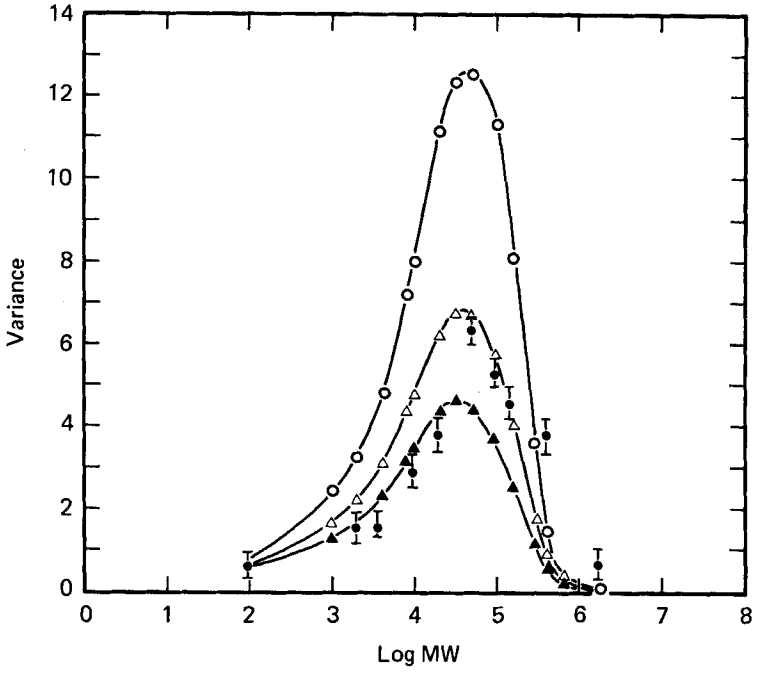

FIG. 6. The existence of a maximum in the variance/molecular weight relationship is predicted by the simulator and verified by experiments. (○) α_s = 1.10, (△) α_s = 1.04, (▲) α_s = 1.00, and (●) experimental points.

weight. This seemingly odd variance–molecular weight relationship becomes self-evident when one considers the currently accepted mechanism of the GPC separation process. The characteristic shape of the variance–molecular weight plot is the result of two opposing molecular-weight-dependent parameters affecting the transport process in and out of the stationary phase. The parameter which tends to increase the band broadening with increasing molecular weight is the diffusion coefficient described by Eqs. (26) and (27). The other parameter which tends to decrease band broadening with increasing molecular weight is the diffusion layer thickness described by Eq. (20). From Eq. (20), the diffusion layer thickness l_s approaches zero as the value of the partition coefficient K approaches unity for solutes with molecular weight (or molecular size) greater than the largest pore of the stationary phase.

Another interesting aspect of Fig. 6 is the agreement between the experiment and the model. It appears that, for molecular weights less than

20,400, the agreement between experiment and model is best when the exponent α_s of Eq. (27) is unity. For the higher molecular weights a better fit is obtained when $\alpha_s = 1.04$. The significance of this behavior is presently unclear. It is, however, tempting to attribute this behavior to some form of weak interaction between the stationary phase and the high molecular weight solute (molecular entanglement?).

Stationary Phase Characteristics and Band Broadening

The practical value of a simulator is that it provides an easy method of investigating the effect of the various chromatographic parameters on the retention volume distribution. For example, the effect of pore size distribution, pore size average, and bead size of the stationary phase can be varied by simply defining these variables in the model. Varying these

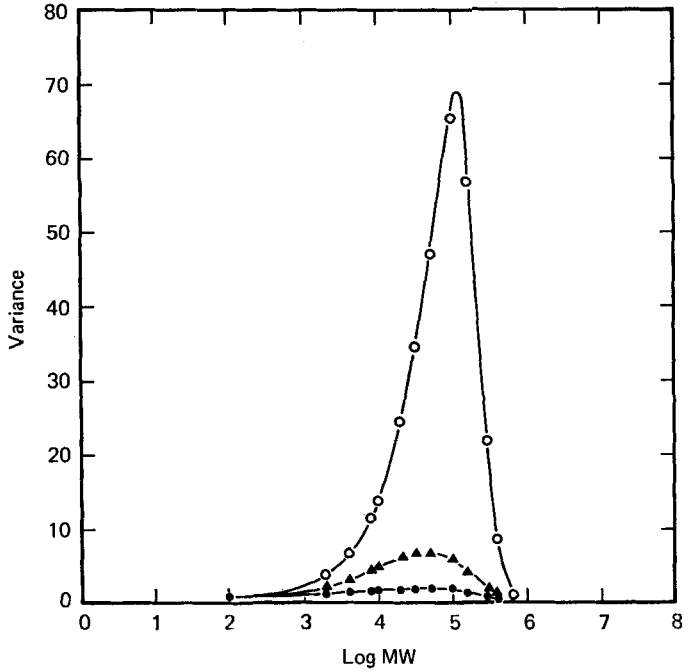

FIG. 7. Broad pore size distribution results in higher retention volume distribution variance than narrow pore size distribution stationary phases. (○) broad pore size distribution beads, (●) narrow pore size distribution beads, and (▲) experimental beads.

parameters experimentally is, at best, a very difficult task. For this work the pore size distribution and pore size average was varied by varying the slope and permeability limit of the calibration curve, respectively, as shown on Fig. 3. Cantow and Johnson (*14*) showed by porosimetry studies that pore size distribution and pore size average can be used to characterize retention volume–molecular size calibration curves.

Figure 7 shows the effect of pore size distribution on band broadening over a wide range of molecular weights. It shows that as the slope of the calibration curve decreases in absolute value (narrowing pore size distribution), the variance of the band increases very rapidly. Although there is a rapid deterioration in the column plate count due to rapid broadening of the peak, it should be pointed out that the separation of component peaks (distances between component peaks) also increases rapidly as evidenced by the calibration curve. The absolute resolution of the column is defined by

$$RE = \frac{(VR_2 - VR_1)}{2(\sigma_1 + \sigma_2)} \tag{29}$$

where VR_2 and VR_1 are the peak retention volumes of Solute 1 and 2, respectively, and the σ's are the standard deviations of the retention volumes. As an illustration, let us compare the resolution of a broad and narrow pore size distribution column for PS-160,000 and PS-97,200 polymers. For the broad pore size distribution column we obtain the following quantities from the model:

$$VR_2 = 37.06, \qquad \sigma_2 = 8.10$$
$$VR_1 = 34.73, \qquad \sigma_1 = 7.56$$
$$RE = 0.075$$

For the narrow pore size distribution, we obtain

$$VR_2 = 26.65, \qquad \sigma_2 = 1.28$$
$$VR_1 = 25.53, \qquad \sigma_1 = 1.15$$
$$RE = 0.230$$

For the medium pore size distribution (actual column used in experiment) we obtain

$$VR_2 = 29.38, \qquad \sigma_2 = 2.40$$
$$VR_1 = 27.46, \qquad \sigma_1 = 2.01$$
$$RE = 2.20$$

The above illustration shows that despite large differences in variances between the narrow and broad pore size distributions (1.63 vs 65.72), their difference in resolution is relatively small (0.23 vs 0.075). Comparing variances and peak separation of the experimental column (packed with stationary phase beads having an intermediate pore size distribution) with the broad and narrow pore size distribution stationary phase beads (hypothetical columns), one can deduce that an optimum pore size distribution may exist such that *RE* is a maximum.

The effect of pore size average on the variance of the band is shown in Fig. 8. The average pore size of the stationary phase is varied by shifting the calibration curve up and down the ordinate while maintaining the slope and pore size distribution constant. It is clear from Fig. 8 that the

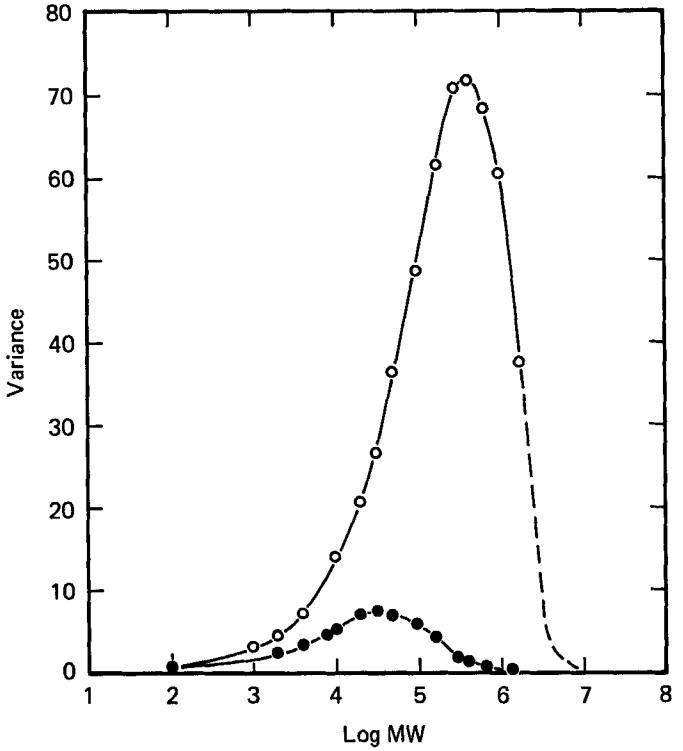

FIG. 8. Large pores result in higher retention volume distribution variance than smaller pore stationary phases. (○) Large pore size average (10^7 permeability limit) and (●) experimental beads (10^4 permeability limit).

variance of the band increases rapidly with increasing pore size average. In addition, the peak of the curve also shifts toward higher molecular weight. Note that the variance of a small molecule, ethylbenzene, is relatively insensitive to changes in the pore size distribution and pore size average, as evidenced by Figs. 7 and 8. This is expected, since small molecules have about 100-fold higher diffusion rates than polymeric solute; consequently, at 1 ml/min flow rate, it will fractionate near equilibrium conditions.

Figures 9 and 10 show the effect of the stationary phase bead size on the shape and width of the retention volume distribution. Again it is evident that the higher molecular weight polymers are more sensitive to changes in bead radius due to their lower diffusion rates. A log-log plot of bead radius vs variance as shown in Fig. 11 illustrates this fact clearly. At very low bead radius, i.e., less than 10 μ, PS-160,000 actually shows lower values of variances. This can be explained as follows: For very small stationary bead particles the diffusion layer becomes very small such that both the polymer and small molecules essentially establish equilibrium between the stationary phase and mobile phase almost instantaneously. Consequently, the band broadening in this region is mainly due to diffusion in the axial direction of the column. Since molecular diffusivities of smaller molecules are higher than larger ones, peak broadening in ethylbenzene is expectably higher when equilibrium between the stationary and mobile phases exists.

Effect of Flow Rate

Figure 12 is an example showing the effect of flow rate on the chromatogram of PS-160,000. As the flow rate increases, the variance and the extent of skewing of the chromatogram also increase. As a consequence of increasing backward skew, the chromatogram peak shifts toward a lower retention volume, since the mean retention volume remains constant (mean retention volume depends only on the partition coefficient K which is held constant).

The dependence of the chromatogram variance on flow rate over a 5-decade range is shown in Fig. 13. For ethylbenzene, equilibrium between the stationary phase essentially exists up to about 0.5 ml/min, while for PS-160,000 equilibrium was not attained until the flow rate was reduced to about 0.01 ml/min. This indicates that diffusion in and out of the stationary phase remains a significant factor of the variance until the value of the $T_D/T_i < 8 \times 10^{-4}$, where T_D and T_i are the time constants

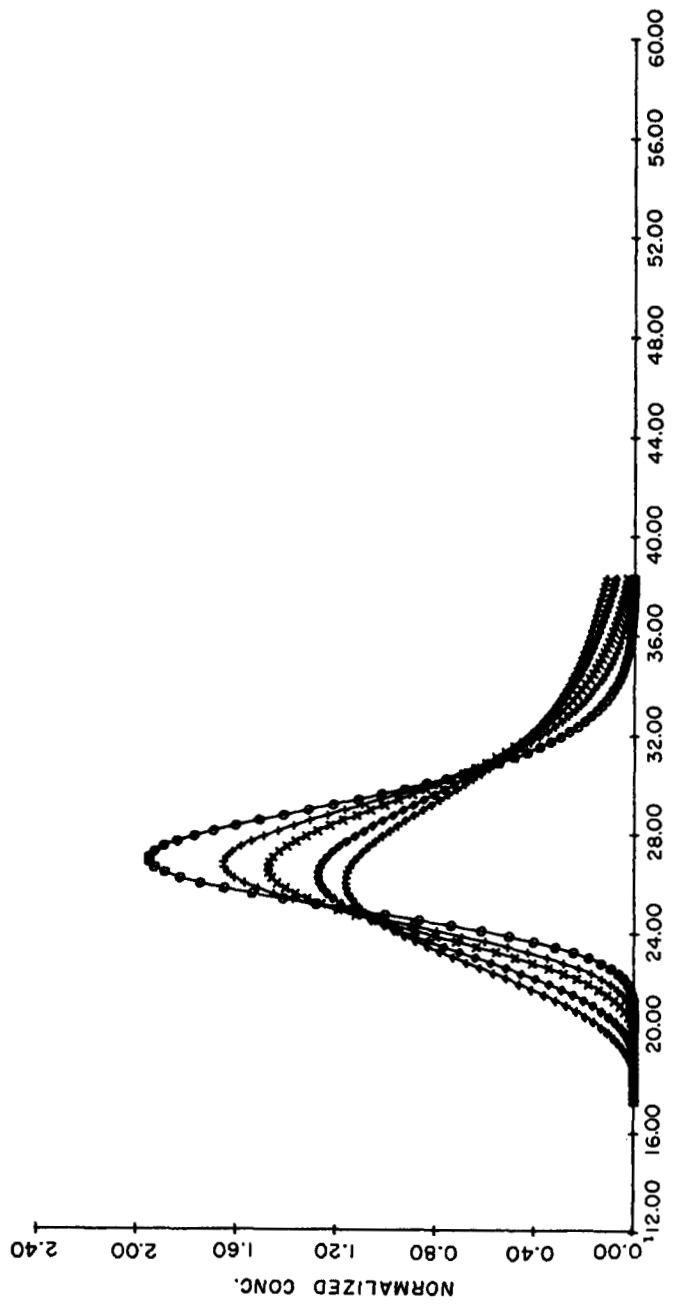

FIG. 9. Peak skewing (tailing) and peak width (square root of variance) increases markedly for PS-160,000 solute with increasing bead radius. (○) 1.5×10^{-3} cm, (▲) 4.5×10^{-3} cm, (+) 2.00×10^{-3} cm, (*) 2.50×10^{-3} cm, and (ϕ) 3.5×10^{-3} cm.

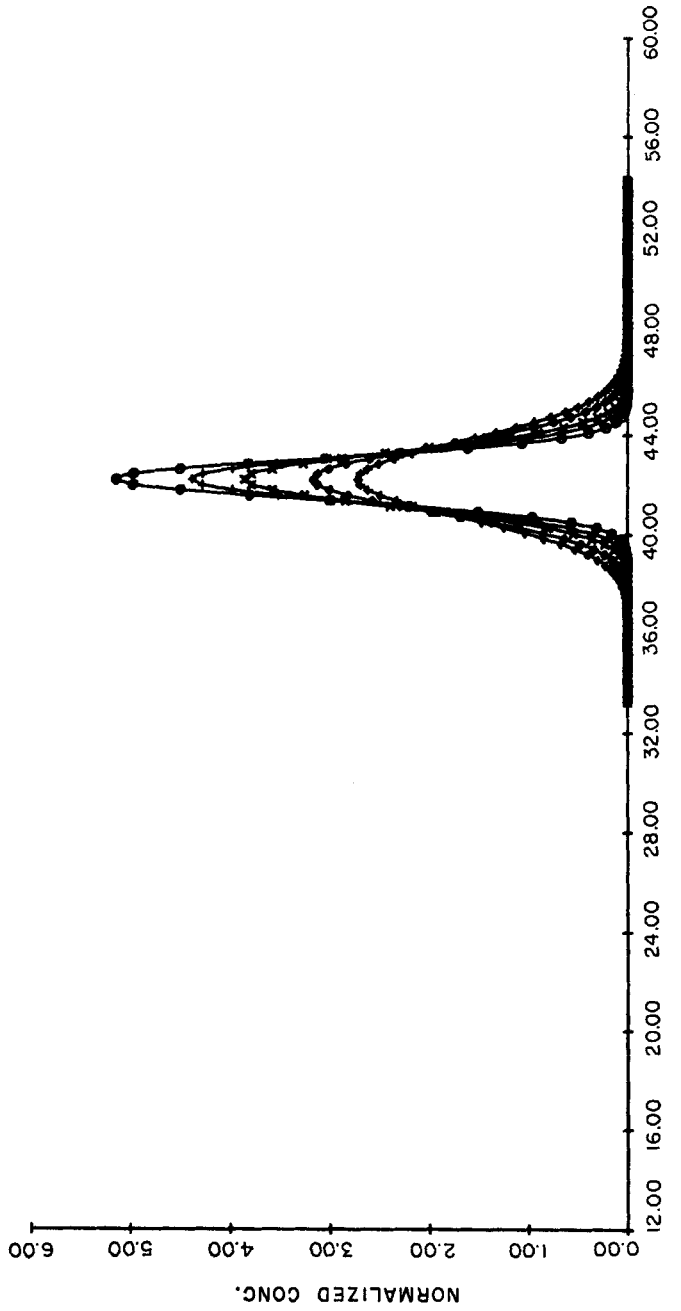

FIG. 10. Peak skewing and peak width also increases with increasing bead radius for ethylbenzene but to a lesser degree than PS-160,000. (○) 1.5×10^{-3} cm, (+) 2.00×10^{-3} cm, (*) 2.5×10^{-3} cm, (ϕ) 3.5×10^{-3} cm, and (▲) 4.5×10^{-3} cm.

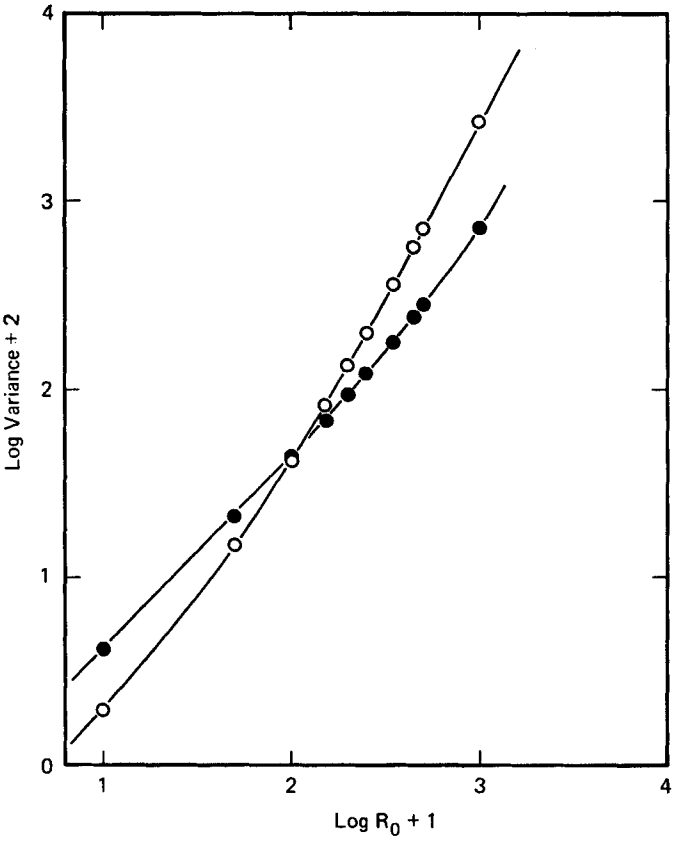

FIG. 11. Peak variance is shown to be strongly dependent on bead radius. The plot shows essentially three regions: equilibrium, transition, and diffusion controlled regions at small ($R_0 < 10\ \mu$), medium ($10\ \mu < R_0 < 100\ \mu$), and large ($R_0 > 100\ \mu$) values of bead radius. (●) Ethylbenzene and (○) PS-160,000.

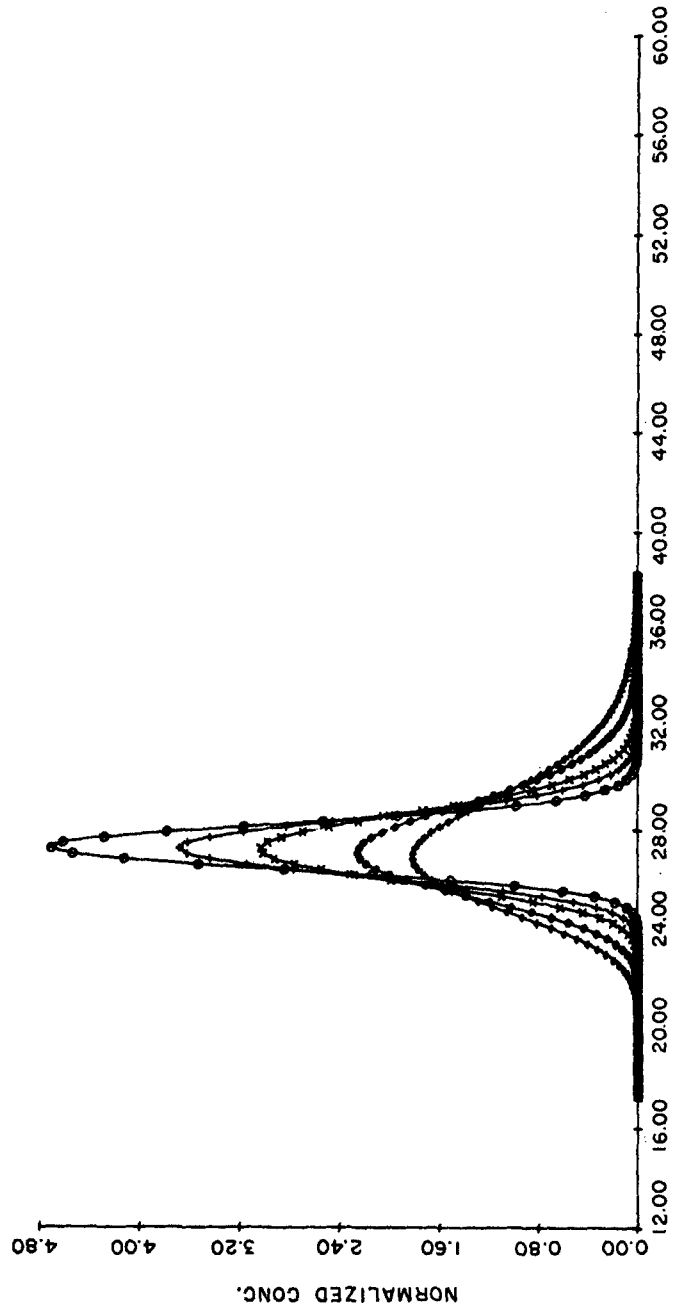

FIG. 12. Flow rate has a very large effect on the shape and width of the retention volume distribution of PS-160,000. (○) 2 ml/min, (+) 3 ml/min, (×) 4 ml/min, (●) 6 ml/min, and (▲) 8 ml/min.

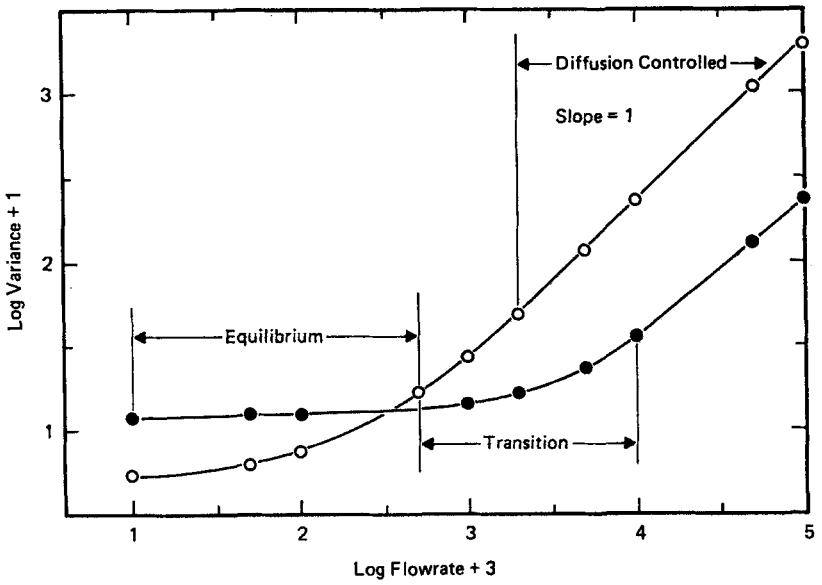

FIG. 13. The square of the peak width (variance) varies with flow rate in three different zones: equilibrium, transition, and diffusion controlled regions. (○) PS-160,000 and (●) ethylbenzene.

for transport through the stationary and mobile phases and average residence times of the polymer in the column, respectively. T_i is defined by Eq. (22) and T_D is defined as

$$T_D = l_s^2/D_s + l_m^2/D_m \tag{30}$$

In the diffusion controlled section of Fig. 13 it is shown that the slope of the plot is equal to unity. This indicates that the width of the band (proportional to the standard deviation σ) varies proportionally with the square root of the flow rate. Experimental values obtained by Little et al. (*15*) showed that the band width varied approximately with the cube root of the flow rate for PS-411,000 in the diffusion-controlled region. This difference may be partly explained by their method of determining band width. The tangent method tends to underestimate band width of peaks with increasing skewedness.

Variance as a function of packing efficiency, λ of Eq. (28), is shown on Fig. 14. Compared to other parameters, the effect of packing efficiency is relatively weak. The variance is seen to be a linear function of λ over a fairly wide range.

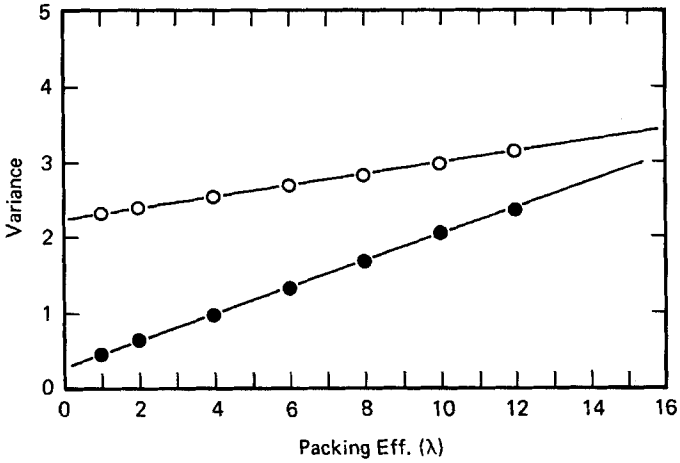

FIG. 14. Variance varies linearly with column packing efficiency λ over a wide range. This relationship assumes no channeling in the packed column. (●) Ethylbenzene and (○) PS-160,000.

CONCLUSION

The results of this work indicate that a phenomenological model solved by the method of moments can simulate the attributes of a GPC chromatogram, i.e., peak shape, mean retention volume, skew, and peak width, provided the velocity profile distortion ("fingering" and channeling) is absent. The simulator can be of considerable value in investigating the effect of various material and experimental parameters on the fractionation behavior of polymers in a GPC column. Consequently, these parameters may be varied to determine experimental conditions which results in optimum resolution for the analysis of polymer molecular weight distribution and the separation or purification of multicomponent systems.

This work demonstrates that at least in GPC the important parameters which determine separation efficiency are the following, listed in a decreasing importance:

(1). Gel pore structure; i.e., shape size distribution and average size.
(2). Gel particle diameter; this controls the diffusion layer thickness of the transport of the solute between the stationary and mobile phases.
(3). Flow rate.

(4). Molecular weight of solute; this affects the diffusion rate in the mobile and stationary phases.

(5). Packing efficiency; this affects axial dispersion due to eddy diffusion and channeling effects.

One aspect of GPC which is not accounted for by this model is the effect of nonuniform velocity profile across the column, which results in forward skewing of GPC chromatograms. This phenomenon has been ascribed to channeling due to the nonuniformity in the stationary phase packing (nonuniform interestitial flow channel). To take this effect into account a more sophisticated model based on a multichannel column representation has been proposed.

Acknowledgments

The authors wish to cite Mr. R. H. McQueen for supplying the SEM photomicrographs shown on Figs. 1 and 1a of this paper. Mr. J. A. Carothers is also cited for his very able technical assistance in obtaining the experimental results presented.

REFERENCES

1. J. C. Giddings and H. Eyring, *J. Phys. Chem.*, *59*, 416 (1955).
2. H. C. Thomas, *J. Amer. Chem. Soc.*, *66*, 1164 (1945).
3. H. C. Thomas, *Ann. N. Y. Acad. Sci.*, *49*, 161 (1948).
4. J. J. Hermans, *J. Polym. Sci.*, *A-2*, *6*, 1217 (1968).
5. J. B. Carmichael, *Ibid.*, *A-2*, *6*, 517 (1968).
6. E. F. Cassasa, *Separ. Sci.*, *6*(2), 305 (1971).
7. E. J. LeFevre, *Nature, Phys. Sci.*, *235*(53), 20 (1972).
8. G. D. Scott, *Nature*, *188*, 908 (1960).
9. J. Brandrup and E. H. Immergut, ed., *Polymer Handbook*, Wiley, New York, 1966.
10. F. Bueche, *Chem. Phys.*, *20*(12), 1956 (1952).
11. A. Klinkenberg and Sjenitzer, *Chem. Eng. Sci.*, *5*, 258 (1956).
12. A. C. Ouano and J. A. Biesenberg, *J. Appl. Polym. Sci.*, *14*, 483 (1970).
13. R. N. Kelley and F. W. Billmeyer, Jr., *Anal. Chem.*, *41*, 874 (1969).
14. M. J. R. Cantow and J. F. Johnson, *J. Polym. Sci.*, *A-1*, *5*, 2835 (1967).
15. J. N. Little, J. L. Waters, K. J. Bambaugh and W. J. Pauplis, *Gel Permeation Chromatography* (K. Altgelt and L. Segal, eds.), 1971, p. 165.

Received by editor May 31, 1973